

Surface chemistry and size influence the release of model therapeutic nanoparticles from poly(ethylene glycol) hydrogels

Stephanie L. Hume · Kavita M. Jeerage

Received: 18 October 2012 / Accepted: 3 April 2013
© Springer Science+Business Media Dordrecht (outside the USA) 2013

Abstract Nanoparticles have emerged as promising therapeutic and diagnostic tools, due to their unique physicochemical properties. The specific core and surface chemistries, as well as nanoparticle size, play critical roles in particle transport and interaction with biological tissue. Localized delivery of therapeutics from hydrogels is well established, but these systems generally release molecules with hydrodynamic radii less than ~ 5 nm. Here, model nanoparticles with biologically relevant surface chemistries and diameters between 10 and 35 nm are analyzed for their release from well-characterized hydrogels. Functionalized gold nanoparticles or quantum dots were encapsulated in three-dimensional poly(ethylene glycol) hydrogels with varying mesh size. Nanoparticle size, surface chemistry, and hydrogel mesh size all influenced the release of particles from the hydrogel matrix. Size influenced nanoparticle release as expected, with larger particles releasing at a slower rate. However, citrate-stabilized gold nanoparticles were not released from hydrogels. Negatively

charged carboxyl or positively charged amine-functionalized quantum dots were released from hydrogels at slower rates than neutrally charged PEGylated nanoparticles of similar size. Transmission electron microscopy images of gold nanoparticles embedded within hydrogel sections demonstrated uniform particle distribution and negligible aggregation, independent of surface chemistry. The nanoparticle-hydrogel interactions observed in this work will aid in the development of localized nanoparticle delivery systems.

Keywords Drug delivery · Gold nanoparticles · Hydrogel · Quantum dots · Surface functionalization

Introduction

Nanoscale therapeutics are rapidly emerging due largely to their ability to enter cells, move through the bloodstream, cross the blood–brain barrier, and carry a high therapeutic payload. Many nanoscale vectors, including viruses, liposomes, and nanoparticles, are capable of effectively transporting drugs or nucleic acids to cells. Nanoparticles, in particular, are an extremely versatile and practical delivery tool, as the properties of their core and shell structures can be independently tailored. This allows for incorporation of both diagnostics and therapeutics, whereby particles are fabricated to enhance imaging contrast or

Contribution of the U.S. Government; not subject to copyright in the United States.

S. L. Hume · K. M. Jeerage (✉)
Applied Chemicals and Materials Division, Material Measurement Laboratory, National Institute of Standards and Technology (NIST), Boulder, CO 80305, USA
e-mail: jeerage@boulder.nist.gov

targeting, simultaneous with controlled release of drugs or nucleic acids. Due to these unique features, nanoparticles have received attention for biosensing and bioimaging, targeted recognition of cancerous cells, and treatment of tumors.

Many early approaches to nanoparticle delivery in a biological environment involve systemic circulation, allowing particle exposure to many cell types and regions of the body (Alexis et al. 2008). Due to the enhanced permeability and retention effect, where macromolecules (Matsumura and Maeda 1986) or nanoparticles (Bartlett et al. 2007) accumulate at higher densities in tumor tissue, this approach has been highly successful for cancer applications. However, achieving the correct therapeutic dosage to an affected area can be difficult. If too many particles are administered systemically they can negatively impact other tissues, whereas too few particles lead to an inadequate dose reaching the affected area. In cases where the target is not a tumor, systemic dosing becomes especially difficult. In these cases, a localized delivery may provide more effective therapy. Localized delivery has been explored for drug release from implantable hydrogel-coated stents (Farb et al. 2001), from implanted hydrogel into bone tissue (Ramchandani and Robinson 1998), or from hydrogels into the injured spinal column (Peralé et al. 2012). As nanoparticle-based therapies evolve, localized drug delivery approaches may need to be redesigned to account for the unique properties of nanomaterials.

We hypothesize that hydrogel platforms previously developed for drug delivery can be effectively translated for use in nanoparticle delivery. Poly(ethylene glycol) (PEG) has been well studied as a polymeric matrix from which biomolecules can be released (Peppas et al. 2000; Lin and Anseth 2009). PEG is bioinert, hydrophilic, and its mesh size can be tuned to manipulate diffusion, and, therefore, release of biomolecules, from the hydrogel network. The release of small dye molecules (Watkins and Anseth 2005), macro- and nano-scale fluorescently tagged spheres (Brandl et al. 2010) and active drugs (Peppas et al. 2000), have been characterized. Although many therapeutic particles are very large (>100 nm), prohibiting their release from most PEG hydrogel systems, nanoparticles would be good candidates for hydrogel release, as proteins with a hydrodynamic radius of less than 10 nm can successfully diffuse through PEG hydrogel networks (Engberg and Frank 2011). Nanoparticle size is expected to

influence diffusion, but surface chemistry should also be considered during design of release, since nanoparticles have uniform surface properties compared to proteins. Depending on physicochemical properties, substantial aggregation is possible, which can influence initial distribution and release from a hydrogel network.

Nanoparticles have been encapsulated or tethered within hydrogel matrices to encourage growth of tissue (Chung et al. 2007), cell transfection (Krebs et al. 2010; Kidd et al. 2012), and improve mechanical properties (Bait et al. 2011; Chang et al. 2010). Mesh size and particle size influence diffusion and release of nanoscale dextrans from PEG hydrogels (Brandl et al. 2010). However, to our knowledge, no previous work has characterized passive release of functionalized nanoparticles where surface chemistry and size can be independently varied. Many particle systems, including gold nanoparticles (AuNPs) or quantum dots (QDs), are amenable to such studies. AuNPs are bioinert, are generally considered non-toxic, and have potential in many therapeutic applications, notably cancer therapies (Llevot and Astruc 2012; Kumar et al. 2012) and as drug delivery systems (Duncan et al. 2010). QDs are intrinsically fluorescent and, therefore, easy to track. Recent advances have improved coatings to make these particles more biocompatible, making medical applications feasible (Azzazy et al. 2007). QDs have been heavily studied as diagnostics, whereby antibodies conjugated to their surfaces target specific cells (Gao et al. 2004; Sukhanova et al. 2012). Theranostics, the incorporation of therapeutics into diagnostics, have employed QDs despite concerns over their long-term toxicity. Although many theranostic systems are composed of large liposomes (several hundred nanometers in diameter), Bagalkot et al. simultaneously conjugated a therapeutic and a targeting function in an outer surface layer surrounding the QD (Bagalkot et al. 2007).

Both bioinert and biologically relevant functional groups are often present at the surface of nanoparticles designed for therapeutic applications. These surfaces can influence release from hydrogel networks, as well as nanoparticle efficacy. PEG and other bioinert surfaces give particles a “stealth” coating (Gref et al. 1994; Owens and Peppas 2006; Otsuka et al. 2003). By minimizing non-specific binding of plasma proteins, thereby blocking macrophage recognition,

stealth coatings lead to longer nanoparticle retention in the bloodstream (Alexis et al. 2008) and may allow penetration of the blood–brain barrier (Calvo et al. 2001; Wohlfart et al. 2012). Bioconjugation of charged molecules, such as amine or carboxyl groups, is a common nanoparticle surface modification in addition to the native particle chemistry or a stealth coating. Often, these groups are incorporated onto the surface in an effort to bind functional drugs (Taylor et al. 2010) or antibodies (Veisoh et al. 2009). Yezhelyev et al. simultaneously conjugated both carboxyl and tertiary amine groups to quantum dots in a successful effort to improve siRNA delivery to cells (Yezhelyev et al. 2008). Promising cancer nanotherapies have emerged through conjugation of drugs with neutral side groups (Dreaden et al. 2009), hydroxyl groups (Hwu et al. 2009; Liu et al. 2010) (Wang et al. 2011), mixed amine and hydroxyl groups (Asadishad et al. 2010; Lu et al. 2012; Mirza and Shamshad 2011), or amine groups only (Taylor et al. 2010) to the nanoparticle surface.

In this work, we designed a PEG hydrogel system such that mesh size could be tailored to be larger than or smaller than the nanoparticle diameter, which was tightly controlled. Nanoparticle release from hydrogels could thus be examined as a function of hydrogel mesh size, as well as nanoparticle diameter. To characterize this model system, three surface coatings and two nanoparticle sizes were investigated. Citrate-stabilized gold nanoparticle reference materials, with diameters of 10 or 30 nm were encapsulated in PEG hydrogels as received, or after conjugation of a PEG layer to their surface. Commercially available QDs with biologically relevant, covalently bound layers of PEG, PEG-carboxyl groups, or PEG-amine groups were also encapsulated within hydrogels. Specific parameters were adjusted in nanoparticle release studies to measure intrinsic properties of the nanoparticles (absorbance for AuNPs and fluorescence for QDs), without the need to incorporate additional markers to detect particles. The specific impact of nanoparticle properties on release from hydrogels was evaluated through measurements of cumulative particle release and hydrogel imaging. Results of this work provide an understanding of the relative importance of surface chemistry and size in directing nanoparticle release from an inert hydrogel matrix, which will aid the design of future localized delivery systems.

Materials and methods¹

Formation of hydrogel networks and characterization of mesh size

Poly(ethylene glycol) dimethacrylate (PEGDM) was synthesized through reaction of methacrylic anhydride with PEG (MW 4600) via microwave methacrylation (Lin-Gibson et al. 2004) in the presence of hydroquinone. Product was dissolved in methylene chloride and then purified by precipitation in ethyl ether. PEGDM was determined to have 95 % of chain ends converted to methacrylate groups, as verified through ¹H NMR. Poly(ethylene glycol) hydrogels were fabricated from aqueous solutions of 5, 7.5, 10, 15, 20, or 30 wt% PEGDM, by adding 0.2 wt% (for 5 wt% macromer solution), 0.08 wt% (for 7.5 wt% macromer solution), or 0.05 wt% (for 10–30 wt% macromer solution) 2-hydroxy-1-[4-(2-hydroxyethoxy)phenyl]-2-methyl-1-propanone photoinitiator (Irgacure 2959, Ciba Specialty Chemicals). Each solution was poured between two glass slides with a 1 mm spacer, and photopolymerized for 5 min on each side under UV light at 365 nm with an intensity of 2 mW/cm² (UVP, model XX-40BLB). Following polymerization, disks 5 mm in diameter were punched from the polymer sheet and then equilibrated in deionized (DI) water for 24 h at room temperature (RT).

Hydrogel disks were weighed swollen (m_s), then lyophilized for 48 h, and weighed dry (m_d) to calculate the equilibrium mass swelling ratio ($q = m_s/m_d$). The equilibrium volumetric swelling ratio (Q) was then calculated by use of the mass swelling ratio and known densities of the uncrosslinked polymer and solvent. The equilibrium polymer volume fraction ($v_{2,s}$ or $1/Q$) was then used to calculate the average molecular weight between crosslinks \bar{M}_c by use of the equation derived by (Flory and Rehner 1943):

$$\frac{1}{\bar{M}_c} = \frac{2}{\bar{M}_n} - \frac{(\bar{v}/V_1)[\ln(1 - v_{2,s}) + v_{2,s} + \chi_{12}v_{2,s}^2]}{[v_{2,s}^{\frac{1}{3}} - \frac{v_{2,s}}{2}]} \quad (1)$$

¹ The full description of the procedures used in this paper requires the identification of certain commercial products and their suppliers. The inclusion of such information should in no way be construed as indicating that such products or supplier are endorsed or recommended by NIST or that they are necessarily the best materials, instruments, software, or suppliers for the purposes described.

The average molecular weight in the absence of crosslinking (\bar{M}_n) does not influence this equation, as the $2/\bar{M}_n$ term is accepted to be negligibly small due to the incorporation of the vast majority of reactive ends into the hydrogel network. In this equation, \bar{v} is the specific volume of the polymer, V_1 is the molar volume of the solvent, and χ_{12} is the solvent–polymer interaction parameter. The average mesh size (ξ) was subsequently determined for each hydrogel composition, using the following relationship between mesh size and hydrogel swelling (Canal and Peppas 1989):

$$\xi = v_{2,s}^{-1/3} C_n^{1/2} l n^{1/2}; \quad (2)$$

where C_n is the characteristic ratio of the polymer, l is the bond length, and n is the number of bonds between crosslinks. A value of 4.0 was used for C_n (Merrill et al. 1993), and l was obtained by averaging the C–C bonds (1.54 Å) and C–O bonds (1.43 Å) found in a repeat unit. To calculate n , \bar{M}_c was divided by the molecular weight of each repeat unit (44 g/mol) and multiplied by the number of bonds in each repeat unit (3).

To estimate nanoparticle diffusivity in the hydrogel, the hydrodynamic radii (r_s) obtained from dynamic light scattering measurements were used in the Stokes–Einstein equation to calculate nanoparticle diffusivity in water (D_o), where k_B is Boltzmann's constant, T is temperature, and η is the viscosity of water:

$$D_o = \frac{k_B T}{6\pi\eta r_s}. \quad (3)$$

The estimated diffusivity in each hydrogel composition (D_g) was then determined by use of a free-volume approach (Lustig and Peppas 1988):

$$\frac{D_g}{D_o} = \left(1 - \frac{r_s}{\xi}\right) \exp\left(-Y \frac{v_{2,s}}{1 - v_{2,s}}\right). \quad (4)$$

The ratio of the critical volume required for translational movement of the solute molecule to the average free volume per molecule of the liquid (Y) is assumed to be unity.

Functionalization and characterization of gold nanoparticles

Citrate-stabilized gold nanoparticles (AuNPs) dispersed in water, with diameters of 10 or 30 nm (NIST

reference material 8011 and 8012, respectively) were used as received, or modified with PEG groups. PEG conjugation was performed by adding 1 mg/mL methoxy-PEG-thiol (MW 1000, Creative PEGworks) to the reference material dispersion, gently shaking, and then reacting for 1 h at RT. Unreacted methoxy-PEG-thiol was removed from the PEG–AuNP product with a stirred ultrafiltration cell (Millipore, model 8003). Dynamic light scattering (DLS) (Zetasizer Nano, Malvern Instruments) was used to evaluate size distribution before and after PEGylation. Measurements were performed at 21 °C and scattered 633 nm light from the helium–neon laser was detected at a 173° scattering angle. Hydrodynamic diameter was reported from the average distribution of particles by volume over 3–6 independent runs. Particle size distributions were verified at multiple timepoints over several weeks, to ensure that the particles were stable. Field emission-scanning electron microscopy (FE-SEM) (LEO 1525, 20 kV) was performed to measure particle diameters before and after PEGylation. To prepare SEM samples, particle suspensions were dropped on a transmission electron microscopy (TEM) grid, and allowed to dry at RT for 3 h.

Nanoparticle encapsulation within hydrogels

Macromer solutions containing 5, 10, or 20 wt% PEGDM and the photoinitiator concentrations described above were used. For citrate-stabilized AuNPs, a constant volume of water was replaced with nanoparticle stock solutions in water. The final macromer solutions had concentrations of 16 µg/mL for 5 wt% hydrogels, 17 µg/mL for 10 wt% hydrogels, and 26 µg/mL for 20 wt% hydrogels. Based on the concentration of reference material stock solutions (50 µg/mL), the maximum concentrations which could have been created if the water used in each formulation was completely replaced with nanoparticle stock solution were 33, 45, and 45 µg/mL, respectively. For PEG–AuNPs, the amount of water replaced in each formulation was adjusted to achieve a constant particle concentration, independent of the hydrogel weight percent. The final macromer solutions had estimated concentrations of 81 µg/mL for 10 nm particles and 162 µg/mL for 30 nm particles. Higher concentrations were due to greater water replacement and to the purification process, in which the volume of the nanoparticle stock solution was

reduced during ultrafiltration (from 5 to 2 mL for 10 nm particles, from 10 to 2 mL for 30 nm particles). These volume changes were used to calculate new stock solution concentrations, neglecting loss to the filter. However, actual stock solution concentrations fall between the initial concentration (50 $\mu\text{g/mL}$) and the maximum concentration based on volume change (125 $\mu\text{g/mL}$ for 10 nm particles and 250 $\mu\text{g/mL}$ for 30 nm particles). For any given stock solution concentration, the hydrogels created had the maximum possible concentration that could be achieved while remaining constant for all three formulations.

To encapsulate QDs, calcium- and magnesium-free phosphate-buffered saline (PBS) was used in place of water to prevent QD aggregation (Koeneman et al. 2009). Quantum dot concentrations of 750 nmol/L were obtained in the final macromer solution by partial replacement of PBS with one of three QD stock solutions: PEGylated QDs with a neutral surface charge (Q21031MP, Invitrogen), functionalized carboxyl QDs with a negative surface charge (Q21331MP, Invitrogen), or functionalized amine QDs with a positive surface charge (Q21531MP, Invitrogen). For PEG-QDs (2 $\mu\text{mol/L}$), the maximum loading is 1300 nmol/L. For COOH-QDs and NH_3 -QDs (8 $\mu\text{mol/L}$), the maximum loading is 5200 nmol/L. Regardless of surface functionalization, all QDs had a cadmium selenide core, zinc sulfide shell, and polymer outer layer (before functionalization). Hydrodynamic diameters, provided by Invitrogen, were reported to be from 14 to 16 nm. Zeta potential measurements in PBS at a concentration of 150 nmol/L in a universal dip cell (ZEN 1002, Malvern) indicated that colloidal stability is highest for COOH-QDs (-26.1 ± 1.1), followed by NH_3 -QDs (-17.0 ± 2.9), and lowest for PEG-QDs (-6.0 ± 1.2). The measured values were significantly different from each other. Each macromer solution was well mixed before 45 μL was added to individual silicon molds 5 mm in diameter and 2 mm deep mounted on a glass slide. Hydrogels were photopolymerized for 10 min on each side under UV light.

Analysis of gold nanoparticle release from hydrogels

Release of citrate-stabilized AuNPs was measured by ultraviolet–visible (UV–Vis) spectroscopy (PerkinElmer LAMBDA 1050). Following polymerization, two hydrogel disks were placed in each DNA LoBind Eppendorf tube containing 200 μL DI water. LoBind tubes were

selected to minimize AuNP adsorption onto the surface. At one of three timepoints (24, 168, and 336 h) the entire solution volume was removed. The absorbance was measured and compared with a standard curve. Separate samples were fabricated for each timepoint. Under these conditions, AuNP release could not be detected, but PEG-AuNP release could be measured.

Release studies with multiple timepoints (4, 24, 96, 168, and 336 h) were designed for PEG-AuNPs only. Following polymerization, two hydrogel disks were placed in each DNA LoBind Eppendorf tube containing 100 μL DI water ($n = 6$). At each timepoint, the solution surrounding the hydrogels was sampled by removing three to five 2 μL aliquots. DI water was added to replace the lost solution volume. Control tubes were prepared with the maximum PEG-AuNP concentration, i.e., the concentration that would exist if all PEG-AuNPs were released from the two hydrogels ($n = 3$), and diluted to create a standard curve (Appendix I). A NanoDropTM 2000 spectrophotometer (Thermo Scientific) was used to measure absorbance of solutions containing 10 nm PEG-AuNPs (522 nm) or 30 nm PEG-AuNPs (529 nm). Sample absorbance was compared to the standard curve and used to determine the cumulative release. Measurement of PEG-AuNP controls remained stable over the time course of the study, for concentrations within the range of the standard curve.

Transmission electron microscopy (TEM) imaging of gold nanoparticle distribution within hydrogels

To visualize the distribution of 10 nm citrate-stabilized or PEGylated AuNPs within 5 wt% PEG hydrogels, hydrogels were exposed to 150 mmol/L mannitol in PBS. Approximately 150- μm -thick slices of the gel were produced manually, immediately loaded into specimen carriers and cryofixed (Wohllwend Compact 02 High Pressure Freezer). The frozen samples were held under liquid nitrogen until freeze-substitution in acetone for 4 days at -80°C . This was followed by low-temperature infiltration with embedding resin (Lowicryl HM20). Finally, the resin was polymerized at -45°C by UV light. Embedded samples were cross-sectioned by ultramicrotome (Leica UC6) to produce sections 100–500 nm thick. Hydrogel cross sections were mounted on TEM grids, and imaged with TEM (JEOL 2000FX, 200 kV) to analyze particle distribution within the hydrogel networks.

Analysis of quantum dot release from hydrogels

Release studies with multiple timepoints (1, 4, 24, 96, and 168 h) were designed. Following polymerization, hydrogel disks were placed in protein LoBind (PEG-QDs and NH_3 -QDs) or DNA LoBind (COOH-QDs) Eppendorf tubes (one gel per tube) containing 350 μL PBS ($n = 5$ or $n = 6$). LoBind tubes were selected to minimize QD adsorption onto the surface. For QD release studies, the entire solution volume was replaced at each sampling timepoint, in contrast to PEG-AuNP release studies where very small volumes were removed. This change in the sampling volume was necessary due to the different measurement techniques required for AuNPs versus QDs. At each QD release timepoint, the hydrogel was gently repositioned to the side, solution was fully removed, and then replaced with fresh PBS. For each experiment, a standard curve was prepared from QDs exposed to UV light during hydrogel polymerization. The fluorescence intensity of samples was read using a plate reader (excitation 485 and emission 560) and concentrations were calculated using the standard curve. For NH_3 -QDs and COOH-QDs, these studies were replicated ($n = 11$ overall).

Epi-fluorescence imaging of quantum dot incorporation and release from hydrogels

Epi-fluorescence measurement of the bulk hydrogels was obtained at each timepoint to qualitatively track changes in QD fluorescence in the bulk hydrogels over time ($n = 2$). For consistent imaging between gels, each image was taken at a focal point 500 μm below the top surface of the gel with an XF302 Qdot 565 filter set (Omega Optical). All images were captured with a constant exposure time of 100 ms. In a separate experiment, hydrogel disks were fabricated as described above, to a 5 wt% composition with no encapsulated particles. Overall hydrogel fluorescence was measured immediately after polymerization, by focusing 500 μm below the top surface of the hydrogel, and imaging with a 20 ms exposure. Hydrogels were then placed in 350 μL PBS (control) or a solution of 230 nmol/L COOH-QDs in PBS. After 48 h, hydrogels were removed and re-imaged. To examine release, hydrogels were placed in 350 μL PBS, and were imaged at 1, 4, 24, 48, and 168 h. At each timepoint, the PBS solution was replaced with 350 μL fresh PBS.

Statistical analysis

Hydrogel properties, nanoparticle diameters, and nanoparticle release percentages from hydrogels were reported as the mean plus or minus one standard deviation. One-way analysis of variation (ANOVA) and the Tukey post-test were used to evaluate the influence of hydrogel wt% or surface chemistry on cumulative nanoparticle release. Differences were considered significant for $p < 0.05$.

Results

Hydrogel mesh size and estimated diffusivity

Mesh size refers to the distance between two adjacent crosslinks, defining the size of openings through which particles can diffuse. Average mesh size was determined through measurements of the swelling properties of various hydrogel compositions in the absence of nanoparticles (Table 1). The 5 wt% hydrogels with the least crosslinking demonstrated the highest volumetric swelling ratio (54), and also the largest mesh size (140 nm). Increasing the weight percentage of PEGDM macromer resulted in a decrease in volumetric swelling ratio and mesh size, where the 30 wt% hydrogel had a mesh size of less than 10 nm. Gold nanoparticles were PEGylated to evaluate the effect of their surface coating on release from hydrogel networks. PEGylation of AuNPs increased their hydrodynamic diameter by nearly 50 % for 10 nm particles (Fig. 1; Table 2) and by about 13 % for 30 nm particles (Table 2). As a result, the estimated diffusion within 5 wt% hydrogels decreased by about 35 % for 10 nm AuNPs and by an order of magnitude for 30 nm AuNPs (Table 2). The range of mesh sizes produced through variation in PEGDM crosslinking density theoretically indicated that all particles would diffuse out of 5 and 10 wt% PEG hydrogels, but only the 10 nm (citrate-stabilized or PEGylated) would diffuse out of 20 wt% PEG hydrogels. Experimentally, however, 10 and 30 nm citrate-stabilized AuNPs became entrapped within the hydrogels, but PEG-AuNPs of both diameters showed varied release from hydrogels, depending on hydrogel mesh size and particle diameter.

Table 1 PEG hydrogel properties determined by Eqs. 1 and 2

PEGDM (wt%)	Volumetric swelling ratio (Q)	Average weight between crosslinks (M_c) (g/mol)	Mesh size (ξ) (nm)
5	54 ± 19	180000 ± 120000	140 ± 54
7.5	23 ± 4	39000 ± 12000	44 ± 9
10	15 ± 1	16000 ± 2500	24 ± 2
15	10 ± 1	7900 ± 1200	15 ± 1
20	8 ± 1	4500 ± 1500	11 ± 2
30	6.5 ± 0.2	2900 ± 190	7.7 ± 0.3

Release of AuNPs and PEG-AuNPs

Citrate-stabilized AuNPs were encapsulated within selected hydrogel compositions (5, 10, and 20 wt%) to first evaluate the effects of nanoparticle size and mesh size on particle release. Encapsulation of citrate-stabilized AuNPs within hydrogels was visually verified, as hydrogels with particles were red, whereas nanoparticle-free hydrogel controls remained transparent (Appendix II). No change in hydrogel color was observed across hydrogel compositions or time, though encapsulated 10 nm particles had a different color than encapsulated 30 nm particles, as expected. Nanoparticle release was monitored by measuring the absorbance of the surrounding solution after one day, one week, or two weeks. No citrate-stabilized AuNPs

were detected. Since this outcome was unexpected, we examined the detection limit in some detail. By adding the quantity of nanoparticles encapsulated in two hydrogels to a solution with a total volume equal to the hydrogel volume plus the water volume, we created a solution with the maximum nanoparticle concentration that would be produced if the gels fully equilibrated. Citrate-stabilized AuNPs in this solution were easily detected and serial dilutions (similar to Appendix I) indicated that 10 % of this concentration could also be detected. To determine whether smaller quantities of citrate-stabilized AuNPs might be released, inductively coupled plasma-mass spectroscopy (ICP-MS) measurements were performed to quantify elemental gold. The control solution described above, representing 10 % of the equilibrated concentration, was easily above the ICP-MS detection limit of 3 ng/mL gold. However, not even the 5 wt% hydrogels released detectable quantities of gold into solution after one week.

PEGylated AuNPs were released from each hydrogel composition over the course of two weeks (Fig. 2), despite a larger diameter than that of citrate-stabilized AuNPs. An initial burst release was observed at early timepoints, followed by a slow release of PEG-AuNPs over a two-week period. Both the hydrogel mesh size and PEG-AuNP diameter contributed to the level of nanoparticle release, where smaller particles encapsulated in a hydrogel network with large mesh size

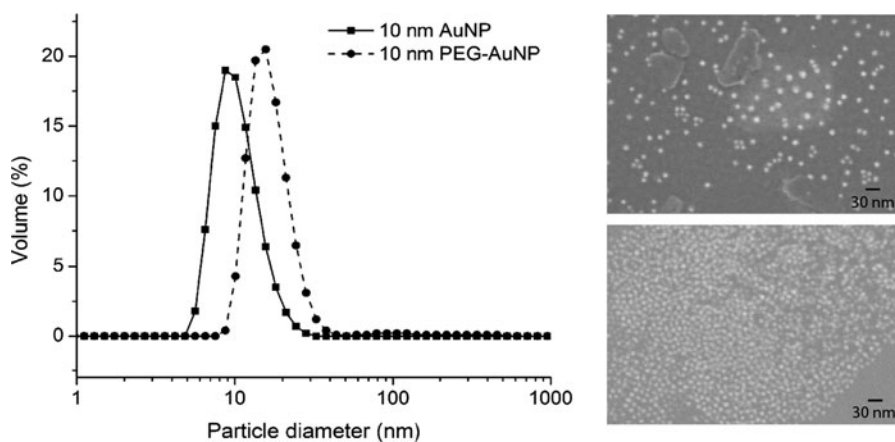


Fig. 1 Volume size distributions show an increase in the hydrodynamic diameter of AuNPs after PEGylation (*left*). AuNPs with a nominal diameter of 10 nm have an average diameter of 11.1 ± 1.8 nm; PEGylation increases the average

diameter to 16.6 ± 0.6 nm. Scanning electron microscopy images of AuNPs (*top right*) and PEG-AuNPs (*bottom right*) do not indicate changes in shape or aggregation. Similar results were obtained for AuNPs with a nominal diameter of 30 nm

Table 2 Diffusivity of AuNPs in PEG hydrogels (D_g) estimated by Eq. 4

Nominal size (nm)	Surface molecules	Hydrodynamic diameter (nm)	D_g 5 wt% PEG ($\mu\text{m}^2 \text{s}^{-1}$)	D_g 10 wt% PEG ($\mu\text{m}^2 \text{s}^{-1}$)	D_g 20 wt% PEG ($\mu\text{m}^2 \text{s}^{-1}$)
10	Citrate	11.1 ± 1.8	38 ± 1	29 ± 1	16 ± 3
10	PEGylated	16.6 ± 0.6	25 ± 1	16 ± 1	4 ± 3
30	Citrate	26.3 ± 0.6	14 ± 1	7 ± 1	–
30	PEGylated	29.7 ± 2.1	1.3 ± 0.1	0.5 ± 0.1	–

released most readily. Small differences, amounting to roughly 5 % of the total encapsulated particles, were observed in PEG-AuNP release between 10 and 20 wt% hydrogels, although release from 10 wt% hydrogels remained higher at each timepoint for both 10 and 30 nm particles. At the conclusion of the study, the 10 and 20 wt% hydrogels had released very similar levels of PEGylated 30 nm AuNPs, amounting to about 15 % of the total encapsulated particles. However, roughly twice as many particles were released from 5 wt% PEG hydrogels than either the 10 or 20 wt% counterparts by the end of the two-week period for both 10 and 30 nm PEGylated AuNPs. As expected, the larger particle size of 30 nm hindered release as compared to the 10 nm particles, allowing release of only 31 % of particles, compared to 65 % of particles, respectively.

Since dramatic differences in release were observed for citrate-stabilized AuNPs compared to PEGylated AuNPs, TEM imaging was performed to compare particle distribution within the hydrogel matrix. Immediately after particle encapsulation, a large number of cross sections (10 to 20) were prepared and examined. Although an occasional aggregate (2 to 3 particles) was observed, nearly all particles existed as individual particles, and no differences were observed between citrate-stabilized AuNPs and PEG-AuNPs (Fig. 3). One week post-encapsulation, hydrogels containing both citrate-stabilized AuNPs and PEG-AuNPs were re-examined and qualitatively found to have no detectable changes in particle density or distribution within the hydrogel (data not shown).

Release of PEG-QDs, NH_3 -QDs, and COOH -QDs

Release of QDs from hydrogels depends on both the mesh size of the hydrogel network, and QD surface functionalization (Fig. 4). The increase in mesh size from 11 ± 2 nm (20 wt% hydrogels) to 24 ± 2 nm

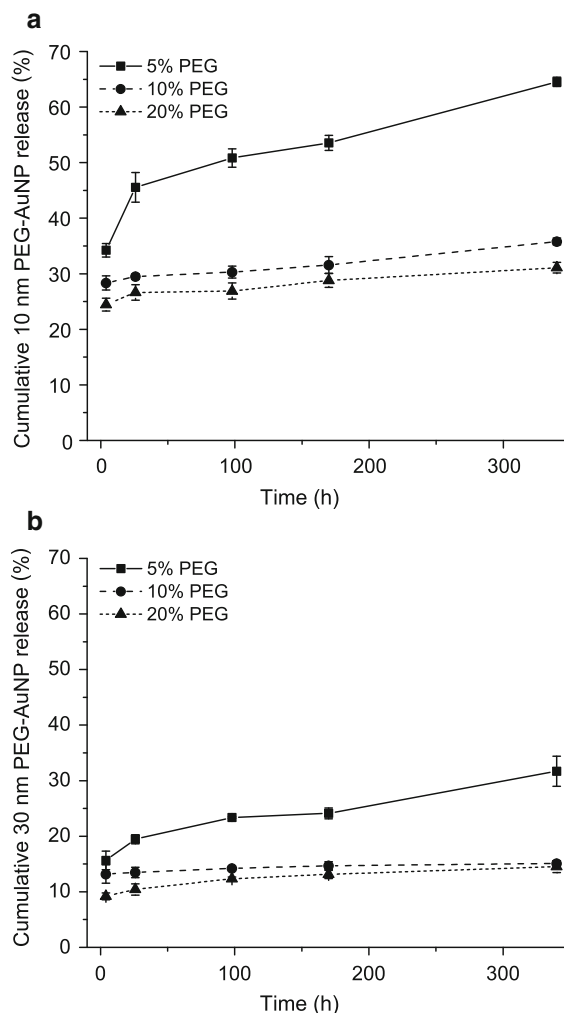


Fig. 2 Cumulative release of 10 nm PEG-AuNPs (**a**) or 30 nm PEG-AuNPs (**b**) was determined at 4, 24, 96, 168, and 336 h following encapsulation. Release was greater from 5 wt% hydrogels than from 10 wt% or 20 wt% hydrogels due to their larger mesh size

(10 wt% hydrogels) yielded only a small increase in QD release from the hydrogels. Both hydrogel compositions retained greater than 85 % of all

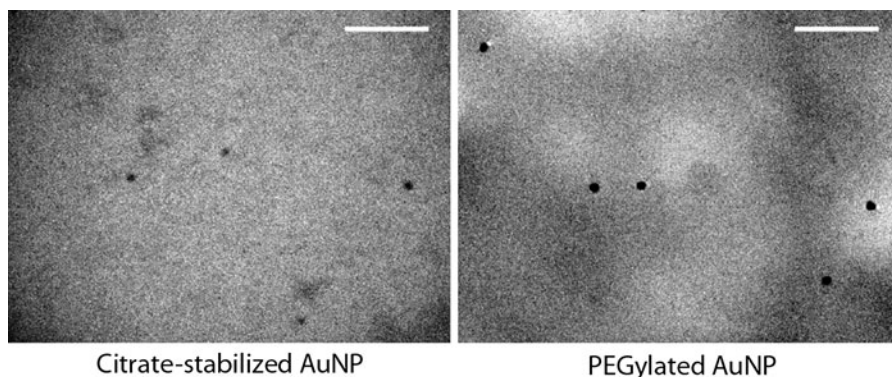


Fig. 3 Transmission electron microscopy cross sections show uniform density and dispersion of 10 nm citrate-stabilized AuNPs or PEG-AuNPs (*black dots*) encapsulated within 5 wt% hydrogels (*gray background*). Scale bar is 100 nm

encapsulated QDs after one week. The larger mesh size of the 5 wt% PEG hydrogels (140 ± 54 nm) allowed a statistically higher release of QDs of all surface chemistries after one week. Although 5 wt% hydrogels allowed the greatest release, QD release was hindered by incorporation of charged surface groups. Release of QDs followed a trend of PEG-QDs > NH_3 -QDs > COOH-QDs over time. While 55 % of neutral, PEG-QDs were released from the 5 wt% hydrogels after one week, the percentage was dramatically reduced to 18 % for positively charged NH_3 -QDs, and 12 % for negatively charged COOH-QDs of the same core/shell composition. The decrease in QD concentration within 5 wt% hydrogels was qualitatively verified through decreases in bulk hydrogel fluorescence (Fig. 5). All hydrogels had similar fluorescence initially (0 h). At 96 h, burst release and subsequent diffusion decreased the intensity of hydrogels with PEG-QDs relative to NH_3 -QDs or COOH-QDs. From 96 to 168 h, diffusion continued to decrease the fluorescence intensity of hydrogels with PEG-QDs, whereas hydrogels with NH_3 -QDs or COOH-QDs did not visually change.

To further evaluate interactions between COOH-QDs and the PEG hydrogel matrix, 5 wt% hydrogels without encapsulated nanoparticles were placed in a COOH-QD solution. COOH-QDs readily diffused into hydrogels over a period of two days, as shown by comparing fluorescence images of COOH-QD-exposed and control hydrogels (Fig. 6). COOH-QD-loaded hydrogels were then placed into PBS under conditions identical to those of the release studies (Fig. 4), with complete solution changes at each

measurement timepoint. Fluorescence decreased after only 1 h and further decreased after 24 h. After 168 h, the fluorescence of exposed hydrogels cannot be distinguished from controls (data not shown). This demonstrates that COOH-QDs introduced into the hydrogel post-polymerization are able to diffuse out of the hydrogel.

Discussion

One advantage of PEG hydrogels for biomedical applications is the ability to control mesh size, leading to manipulation of biomolecule release. The cross-linking density of PEG hydrogels formed through radical-initiated polymerization can be tuned through changes to the PEG weight percentage, although it can also be dramatically influenced by the PEG molecular weight (Cruise et al. 1998). This study used changes in PEG weight percentage to create mesh sizes that varied over an order of magnitude. This wide range made it possible to design release studies with hydrogel mesh sizes (11, 24, and 140 nm, Table 1) relevant to nanoparticles between 10 and 35 nm in diameter. One caveat is that while this approach does produce large mesh sizes (5 wt% hydrogels), they can be due to imperfections in the polymerization, such as unreacted ends or cyclization, rather than exclusively to the formation of uniformly large pores. For all particles studied here with measurable release from PEG hydrogels, an initial burst release was followed by slow nanoparticle release over time, dictated by the average hydrogel mesh size. Particles released in the

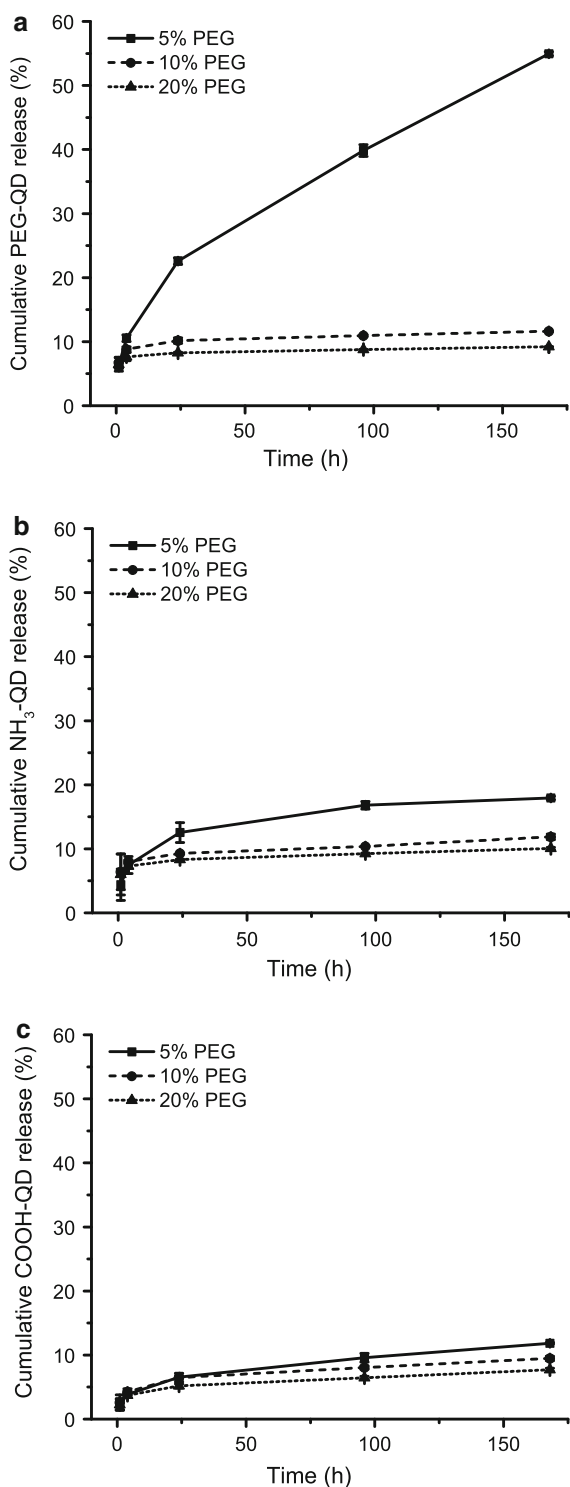


Fig. 4 Cumulative release of 14-nm-diameter PEG-QDs (a), NH₃-QDs (b), or COOH-QDs (c) was determined at 1, 4, 24, 96, and 168 h following encapsulation. Release from 5 wt% hydrogels followed the sequence PEG-QDs > NH₃-QDs > COOH-QDs

initial “burst” were located near the edges of the hydrogel and were not completely incorporated into the network, possibly due to oxygen inhibition of the PEG polymerization at the air–polymer interface. As seen in similar studies of protein release, the burst release is influenced by mesh size, with a large mesh (5 wt%) producing a significantly greater release than a tight mesh (20 wt%), for 10 and 30 nm PEG-AuNPs (Fig. 2). Following the burst release, 10 and 30 nm PEG-AuNPs continue to diffuse from 5 wt% hydrogels. However, 10 and 20 wt% hydrogels release only small additional amounts (less than 8 % cumulative release after two weeks). The decrease in nanoparticle release resulting from a decrease in the tailored hydrogel mesh size was expected for our studies.

Although absorbance is a well-established approach for quantifying AuNPs in solution, relatively high concentrations are required. Due to limitations on the concentration of initial nanoparticle suspensions, nanoparticles were not packed at high densities into hydrogels (Fig. 3). As a result, the surrounding solution volume was relatively low as a prerequisite for obtaining accurate measurements of AuNPs in solution. With this approach, true sink conditions were not present during release, and the release of approximately 50 % of the encapsulated particles would indicate equilibration. As expected, 30 nm PEG-AuNPs were released from hydrogels of identical average mesh at a slower rate than that for 10 nm PEG-AuNPs (Fig. 2). However, 10 nm PEG-AuNPs may have reached equilibrium at the 96-h timepoint. Subsequent partial solution changes would then allow only small additional release, as observed. Since far less of the 30 nm PEG-AuNPs were released over the same time period, this system was likely not close to equilibrium. Instead, release was hindered by size restrictions on particle diffusion out of the hydrogel network based on the relationship between particle size and mesh size. One potential confounding factor is that PEG hydrogel networks may be distorted by encapsulation of particles (e.g., cells) (Cho et al. 2009). Although this impact would be lessened with the far smaller nanoparticles, it could impact release of 30 nm particles slightly more than 10 nm particles.

Other systems that encapsulate nanoparticles in hydrogels have observed particle release, either by design, or as a side product, while enhancing biological function or mechanical strength. Generally, this

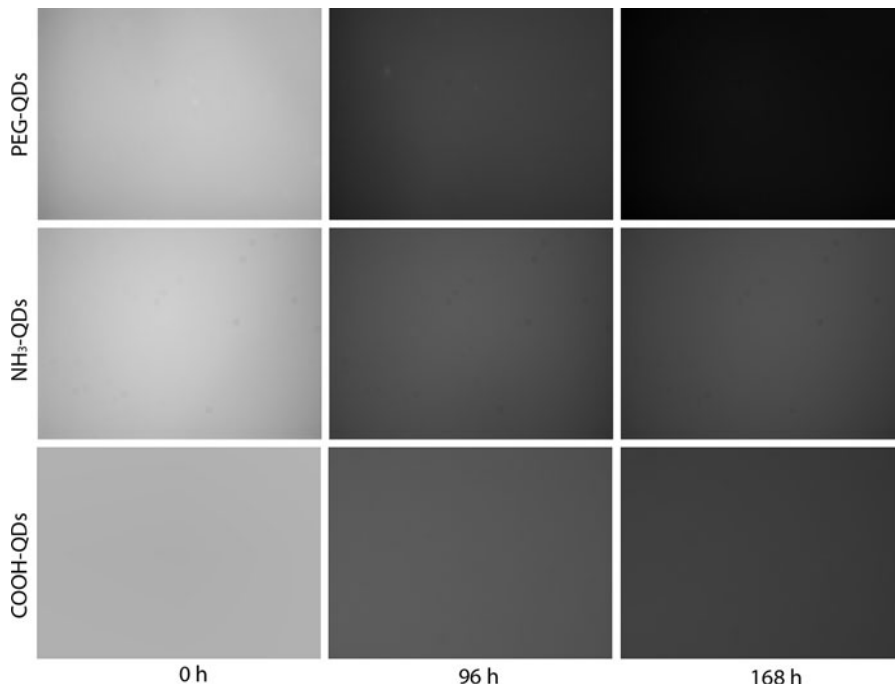


Fig. 5 Differences in the release of surface-functionalized QDs from 5 wt% hydrogels were visually verified by fluorescence microscopy. Acquisition conditions and intensity scale are identical for all images

passive diffusion of large molecules is attributed to size compatibility between the matrix and solute. In fact, previous work has verified a size-dependent release of spherical particles of 3, 8, and 33 nm from crosslinked PEG hydrogels (Brandl et al. 2010). However, other research indicates that effects of additional physicochemical properties may influence diffusion through a hydrogel matrix. Often, these

effects cannot be independently examined, as no mechanisms other than size exclusion are tested.

Our platform affords the ability to independently examine the effects of size and surface functionalization on release of nanoparticles from hydrogel networks. Comparing PEG-AuNPs, PEG-QDs, NH₃-QDs, and COOH-QDs within the same PEG hydrogel compositions allowed for analysis of surface chemistry effects

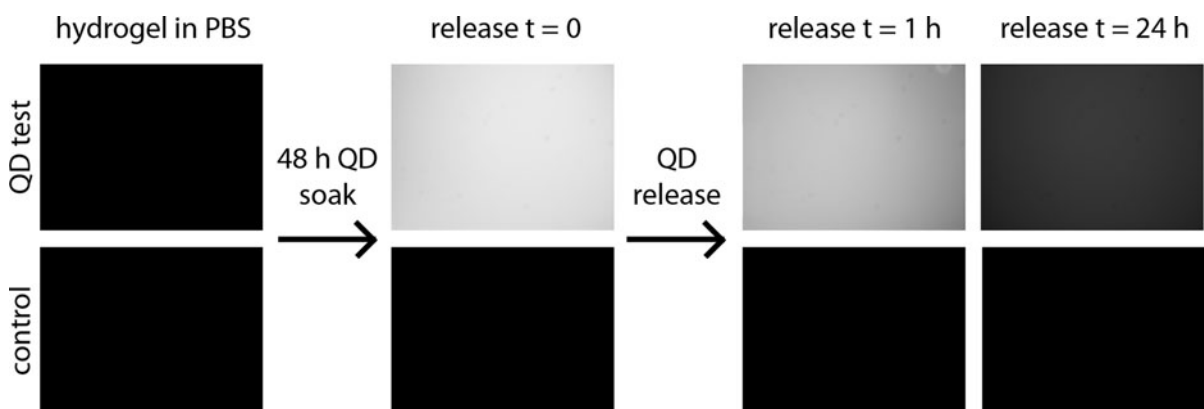


Fig. 6 Hydrogels (5 wt%) were imaged immediately after polymerization in PBS (1st column), soaked in COOH-QD solution (*top*) or PBS (*bottom*), and then re-imaged (2nd column). Hydrogels were then placed in PBS solution and

COOH-QD release was tracked by fluorescence imaging (*top images*) and compared with controls which remained in PBS solution (*bottom images*). Acquisition conditions and intensity scale are identical for all images

between particles of very similar hydrodynamic diameter. Comparing release of the three types of QDs from 5 wt% hydrogels, an initial burst release was first observed, as already described. However, the burst measured at the 1-h timepoint also varied with surface chemistry, with COOH-QDs significantly lower than PEG-QDs or NH₃-QDs. By the 24-h timepoint, the release rates could be clearly differentiated, and followed the trend PEG-QD > NH₃-QD > COOH-QD, with the COOH-QDs barely releasing above the burst levels. Although Invitrogen's reported hydrodynamic diameters (14–16 nm) varied from other published data (Ryman-Rasmussen et al. 2006), where hydrodynamic diameters were reported to be 14 nm for COOH-QDs, 15 nm for NH₃-QDs, and 35 nm for PEG-QDs, the much greater release of PEG-QDs in our system indicated that any size discrepancy was not the governing factor. Further, the measured zeta potentials indicated less colloidal stability for PEG-QDs. Together, this evidence suggests that surface chemistry was the dominant factor in QD release from our hydrogel system.

This was especially interesting because the citrate-stabilized AuNPs had no measureable release, even from 5 wt% hydrogels during initial burst phase. When the citrate-stabilized AuNPs were encapsulated in hydrogels, no release could be detected through UV–Vis. In an effort to detect very low levels of release, ICP-MS was performed. Despite the low detection limit for elemental gold, no gold could be measured in the solution surrounding 5 wt% hydrogel samples after a burst release, or after one week. Interestingly, once the particles were functionalized with a PEG layer and encapsulated using the same procedure, PEG-AuNPs could easily be detected in solution after only 4 h of release from hydrogels, despite the size increase due to PEGylation.

The limited or undetectable release of NH₃-QDs, COOH-QDs, and citrate-stabilized AuNPs from 5 wt% hydrogels indicates some mechanism of retention of charged particles within the hydrogel network. It was first hypothesized that nanoparticle entrapment might be due to clustering of the particles in the polymer precursor solution. Aggregation of particles within the hydrogel network would likely trap particles permanently, since aggregates would be larger than the mesh size for any of the hydrogel networks examined in this study. Particles would be unlikely to dissociate from the aggregates to diffuse out over time, due to the strength of the particle–particle interactions that

caused initial aggregation. TEM imaging of 5 wt% hydrogels showed that both citrate-stabilized AuNPs (which do not diffuse) and PEG-AuNPs (which do) were encapsulated with uniform distribution throughout the hydrogel. Hydrogel sections imaged after one week were similar. This observation suggests that aggregation was not primarily responsible for retention of citrate-stabilized AuNPs within hydrogel networks.

There is evidence that citrate-stabilized AuNPs can interact with the hydrogel networks through hydrogen bonding. This phenomenon was observed when polyacrylamide gels were formed, shrunken in acetone, and then swollen in an aqueous solution containing suspended, citrate-stabilized gold nanoparticles. Upon subsequent solvent changes, AuNPs remained inside the hydrogel network (Pardo-Yissar et al. 2001). PEG hydrogel interactions with charged nanoparticles could account for the lower burst release of charged particles from hydrogels observed in our studies. In this case, particles may continue to interact with PEG chains even if they are not completely entrapped in the hydrogel network.

The retention of charged particles within the hydrogel network may instead be tied to interactions with the macromer solution during polymerization. Thiol groups incorporated into macromer solutions are capable of reacting with the surface of AuNPs (Phillips et al. 2008), but there is little evidence suggesting a strong interaction between methacrylate groups and the gold surface. Although a clear tethering mechanism was not identified for bonding charged particles within the hydrogel network, the ability of COOH-QDs to diffuse into hydrogels after polymerization, and subsequently diffuse out (Fig. 6), suggests that some retention of particles in the release systems studied was due to interactions between the charged particle surface and macromer or initiator radicals during the polymerization process.

These findings will be critical to the design of applications requiring nanoparticles with bioactive surfaces to interact with PEG hydrogels. For example, QDs functionalized with negatively charged surface groups (including COOH groups) are endocytosed by cells (Ryman-Rasmussen et al. 2007; Delehanty et al. 2009). Delivering such particles would require loading the hydrogel post-polymerization. However, it could extend further to frequently studied protein or nucleic acid release from hydrogel systems (Quick and Anseth 2004; Lei et al. 2010). While such therapeutics often

contain surface charges, the effect of their charges on retention or release from a hydrogel network cannot be independently studied. This work provides a method to analyze surface charge effects in conjunction with size effects in designing delivery systems. The information gained from this study could alternatively be important to applications such as tissue engineering, where permanent encapsulation and retention of nanoparticles is desired within a hydrogel matrix.

Conclusion

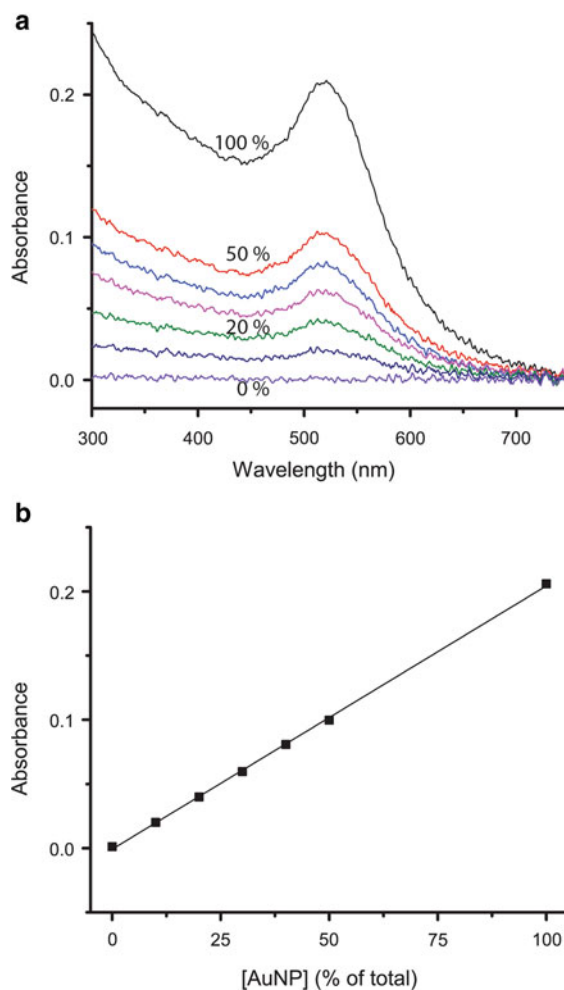
While PEG hydrogels have been extensively studied for delivery of therapeutic biomolecules, the release of core-shell nanoparticles has not been previously examined as a function of nanoparticle physicochemical properties, in particular, diameter and surface molecules. Here, nanoparticles of varied diameter, core composition, and surface chemistry were encapsulated within well-characterized PEG hydrogels fabricated with a range of mesh sizes. Release of neutral, PEGylated nanoparticles depended on size. However, functionalization with positively charged amine groups, negatively charged carboxyl groups, or citrate stabilization dramatically reduced nanoparticle release from all hydrogel compositions. Inspection of AuNPs within the hydrogel network through TEM imaging suggested that charged particle entrapment within the PEG network was not due to particle aggregation during encapsulation, but was likely based on interactions between the charged particles and the hydrogel network. Loading and release of COOH-QDs suggest that these charged particles are tethered into the hydrogel during polymerization. These studies will lay a foundation for development of future nanoparticle delivery systems from hydrogel networks.

Acknowledgments The authors acknowledge Dr. Roy Geiss for his assistance with TEM imaging, Dr. Tom Giddings for his assistance with hydrogel sectioning, and Dr. John Drexler for his assistance with ICP-MS. The authors also thank the National Research Council (NRC) and the American Recovery and Reinvestment Act for a post-doctoral fellowship to SLH.

Appendix I

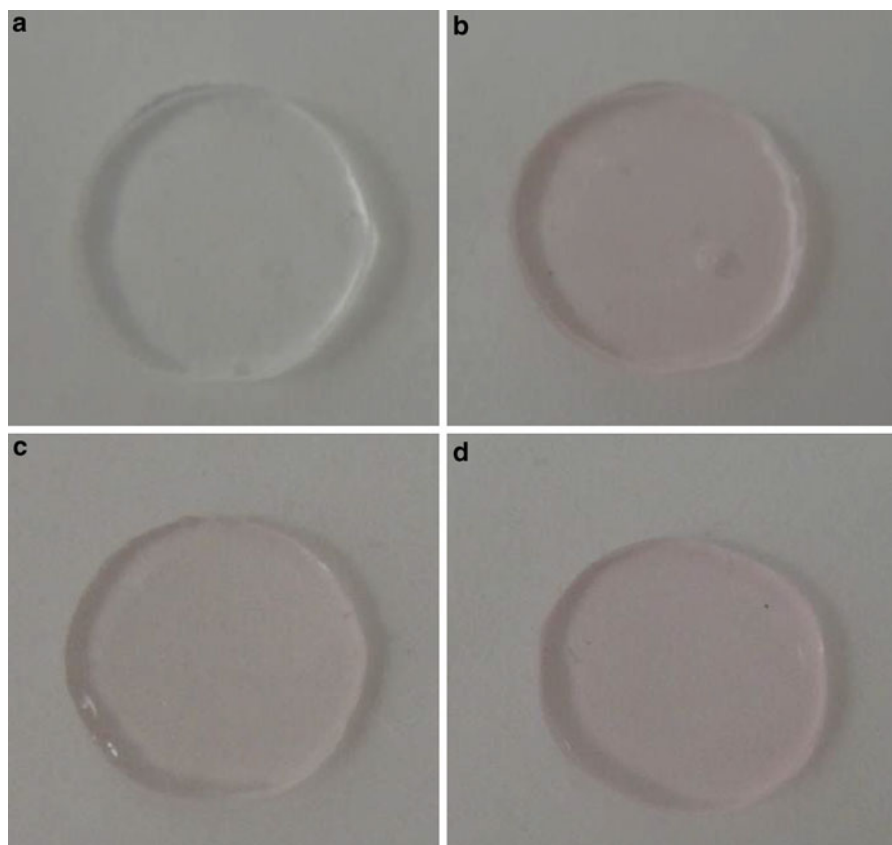
UV-Vis absorbance decreases as the 10 nm PEG-AuNP stock solution is diluted (a). Calibration curves were

constructed from the absorbance peak at 522 nm for each corresponding percentage of original stock solution (b), and used to determine PEG-AuNPs released into solution. Similar results were obtained for 30 nm PEG-AuNP stock solutions and calibration curves were constructed from the absorbance peak at 529 nm.



Appendix II

In the absence of gold nanoparticles, PEG hydrogels are translucent (a). Upon encapsulation of AuNPs, the hydrogel is pink through visual inspection (b). Although slight changes in color result from differences in encapsulated nanoparticle size, both encapsulated 10 nm AuNPs (c) and 30 nm AuNPs (d) remain embedded in a 5 wt% hydrogel after 7 d



immersed in water, and look visually the same as immediately after polymerization.

References

- Alexis F, Pridgen E, Molnar LK, Farokhzad OC (2008) Factors affecting the clearance and biodistribution of polymeric nanoparticles. *Mol Pharmaceut* 5(4):505–515. doi:[10.1021/Mp800051m](https://doi.org/10.1021/Mp800051m)
- Asadishad B, Vossoughi M, Alemzadeh I (2010) Folate-receptor-targeted delivery of doxorubicin using polyethylene glycol-functionalized gold nanoparticles. *Ind Eng Chem Res* 49(4):1958–1963. doi:[10.1021/Te9011479](https://doi.org/10.1021/Te9011479)
- Azzazy HME, Mansour MMH, Kazinierczak SC (2007) From diagnostics to therapy: prospects of quantum dots. *Clin Biochem* 40(13–14):917–927. doi:[10.1016/j.clinbiochem.2007.018](https://doi.org/10.1016/j.clinbiochem.2007.018)
- Bagalkot V, Zhang L, Levy-Nissenbaum E, Jon S, Kantoff PW, Langer R, Farokhzad OC (2007) Quantum dot—aptamer conjugates for synchronous cancer imaging, therapy, and sensing of drug delivery based on Bi-fluorescence resonance energy transfer. *Nano Lett* 7(10):3065–3070. doi:[10.1021/Nl071546n](https://doi.org/10.1021/Nl071546n)
- Bait N, Grassl B, Deraill C, Benaboura A (2011) Hydrogel nanocomposites as pressure-sensitive adhesives for skin-contact applications. *Soft Matter* 7(5):2025–2032. doi:[10.1039/c0sm01123a](https://doi.org/10.1039/c0sm01123a)
- Bartlett DW, Su H, Hildebrandt IJ, Weber WA, Davis ME (2007) Impact of tumor-specific targeting on the biodistribution and efficacy of siRNA nanoparticles measured by multimodality in vivo imaging. *Proc Natl Acad Sci USA* 104(39):15549–15554. doi:[10.1073/pnas.0707461104](https://doi.org/10.1073/pnas.0707461104)
- Brandl F, Kastner F, Gschwind RM, Blunk T, Tessmar J, Gopferich A (2010) Hydrogel-based drug delivery systems: comparison of drug diffusivity and release kinetics. *J Control Release* 142(2):221–228. doi:[10.1016/j.jconrel.2009.10.030](https://doi.org/10.1016/j.jconrel.2009.10.030)
- Calvo P, Gouritin B, Chacun H, Desmaele D, D'Angelo J, Noel JP, Georgin D, Fattal E, Andreux JP, Couvreur P (2001) Long-circulating PEGylated polycyanoacrylate nanoparticles as new drug carrier for brain delivery. *Pharm Res* 18(8):1157–1166
- Canal T, Peppas NA (1989) Correlation between mesh size and equilibrium degree of swelling of polymeric networks. *J Biomed Mater Res* 23(10):1183–1193
- Chang CW, van Spreeuwel A, Zhang C, Varghese S (2010) PEG/clay nanocomposite hydrogel: a mechanically robust tissue engineering scaffold. *Soft Matter* 6(20):5157–5164. doi:[10.1039/c0sm00067a](https://doi.org/10.1039/c0sm00067a)
- Cho NJ, Elazar M, Xiong AM, Lee W, Chiao E, Baker J, Frank CW, Glenn JS (2009) Viral infection of human progenitor and liver-derived cells encapsulated in three-dimensional PEG-based hydrogel. *Biomed Mater* 4(1):011001. doi:[10.1088/1748-6041/4/1/011001](https://doi.org/10.1088/1748-6041/4/1/011001)

- Chung YI, Ahn KM, Jeon SH, Lee SY, Lee JH, Tae G (2007) Enhanced bone regeneration with BMP-2 loaded functional nanoparticle-hydrogel complex. *J Control Release* 121(1–2):91–99. doi:[10.1016/j.jconrel.2007.05.029](https://doi.org/10.1016/j.jconrel.2007.05.029)
- Cruise GM, Scharp DS, Hubbell JA (1998) Characterization of permeability and network structure of interfacially photopolymerized poly(ethylene glycol) diacrylate hydrogels. *Biomaterials* 19(14):1287–1294
- Delehanty JB, Mattoussi H, Medintz IL (2009) Delivering quantum dots into cells: strategies, progress and remaining issues. *Anal Bioanal Chem* 393(4):1091–1105. doi:[10.1007/s00216-008-2410-4](https://doi.org/10.1007/s00216-008-2410-4)
- Dreaden EC, Mwakwari SC, Sodji QH, Oyelere AK, El-Sayed MA (2009) Tamoxifen-poly(ethylene glycol)-thiol gold nanoparticle conjugates: enhanced potency and selective delivery for breast cancer treatment. *Bioconjugate Chem* 20(12):2247–2253. doi:[10.1021/Bc9002212](https://doi.org/10.1021/Bc9002212)
- Duncan B, Kim C, Rotello VM (2010) Gold nanoparticle platforms as drug and biomacromolecule delivery systems. *J Control Release* 148(1):122–127. doi:[10.1016/j.jconrel.2010.06.004](https://doi.org/10.1016/j.jconrel.2010.06.004)
- Engberg K, Frank CW (2011) Protein diffusion in photopolymerized poly(ethylene glycol) hydrogel networks. *Biomed Mater* 6(5):055006. doi:[10.1088/1748-6041/6/5/055006](https://doi.org/10.1088/1748-6041/6/5/055006)
- Farb A, Heller PF, Shroff S, Cheng L, Kolodgie FD, Carter AJ, Scott DS, Froehlich J, Virmani R (2001) Pathological analysis of local delivery of paclitaxel via a polymer-coated stent. *Circulation* 104(4):473–479. doi:[10.1161/hc3001.092037](https://doi.org/10.1161/hc3001.092037)
- Flory PJ, Rehner J (1943) Statistical mechanics of cross-linked polymer networks I rubberlike elasticity. *J Chem Phys* 11(11):512–520
- Gao XH, Cui YY, Levenson RM, Chung LWK, Nie SM (2004) In vivo cancer targeting and imaging with semiconductor quantum dots. *Nat Biotechnol* 22(8):969–976. doi:[10.1038/Nbt994](https://doi.org/10.1038/Nbt994)
- Gref R, Minamitake Y, Peracchia MT, Trubetskoy V, Torchilin V, Langer R (1994) Biodegradable long-circulating polymeric nanospheres. *Science* 263(5153):1600–1603
- Hwu JR, Lin YS, Josephrajn T, Hsu MH, Cheng FY, Yeh CS, Su WC, Shieh DB (2009) Targeted paclitaxel by conjugation to iron oxide and gold nanoparticles. *J Am Chem Soc* 131(1):66–68. doi:[10.1021/Ja804947u](https://doi.org/10.1021/Ja804947u)
- Kidd ME, Shin S, Shea LD (2012) Fibrin hydrogels for lentiviral gene delivery in vitro and in vivo. *J Control Release* 157(1):80–85. doi:[10.1016/j.jconrel.2011.08.036](https://doi.org/10.1016/j.jconrel.2011.08.036)
- Koenenman BA, Zhang Y, Hristovski K, Westerhoff P, Chen YS, Crittenden JC, Capco DG (2009) Experimental approach for an in vitro toxicity assay with non-aggregated quantum dots. *Toxicol In Vitro* 23(5):955–962. doi:[10.1016/j.tiv.2009.05.007](https://doi.org/10.1016/j.tiv.2009.05.007)
- Krebs MD, Salter E, Chen E, Sutter KA, Alsberg E (2010) Calcium alginate phosphate-DNA nanoparticle gene delivery from hydrogels induces in vivo osteogenesis. *J Biomed Mater Res Part A* 92A(3):1131–1138. doi:[10.1002/jbm.a.32441](https://doi.org/10.1002/jbm.a.32441)
- Kumar A, Ma HL, Zhang X, Huang KY, Jin SB, Liu J, Wei T, Cao WP, Zou GZ, Liang XJ (2012) Gold nanoparticles functionalized with therapeutic and targeted peptides for cancer treatment. *Biomaterials* 33(4):1180–1189. doi:[10.1016/j.biomaterials.2011.10.058](https://doi.org/10.1016/j.biomaterials.2011.10.058)
- Lei YG, Huang SX, Sharif-Kashani P, Chen Y, Kavehpour P, Segura T (2010) Incorporation of active DNA/cationic polymer polyplexes into hydrogel scaffolds. *Biomaterials* 31(34):9106–9116. doi:[10.1016/j.biomaterials.2010.08.016](https://doi.org/10.1016/j.biomaterials.2010.08.016)
- Lin CC, Anseth KS (2009) PEG hydrogels for the controlled release of biomolecules in regenerative medicine. *Pharm Res* 26(3):631–643. doi:[10.1007/s11095-008-9801-2](https://doi.org/10.1007/s11095-008-9801-2)
- Lin-Gibson S, Bencherif S, Cooper JA, Wetzel SJ, Antonucci JM, Vogel BM, Horkay F, Washburn NR (2004) Synthesis and characterization of PEG dimethacrylates and their hydrogels. *Biomacromolecules* 5(4):1280–1287. doi:[10.1021/Bm0498777](https://doi.org/10.1021/Bm0498777)
- Liu KK, Zheng WW, Wang CC, Chiu YC, Cheng CL, Lo YS, Chen CP, Chao JI (2010) Covalent linkage of nanodiamond-paclitaxel for drug delivery and cancer therapy. *Nanotechnology* 21(31):315106. doi:[10.1088/0957-4484/21/31/315106](https://doi.org/10.1088/0957-4484/21/31/315106)
- Llevot A, Astruc D (2012) Applications of vectorized gold nanoparticles to the diagnosis and therapy of cancer. *Chem Soc Rev* 41(1):242–257. doi:[10.1039/c1cs15080d](https://doi.org/10.1039/c1cs15080d)
- Lu YJ, Wei KC, Ma CCM, Yang SY, Chen JP (2012) Dual targeted delivery of doxorubicin to cancer cells using folate-conjugated magnetic multi-walled carbon nanotubes. *Colloid Surface B* 89:1–9. doi:[10.1016/j.colsurfb.2011.08.001](https://doi.org/10.1016/j.colsurfb.2011.08.001)
- Lustig SR, Peppas NA (1988) Solute diffusion in swollen membranes. 9. Scaling laws for solute diffusion in gels. *J Appl Polym Sci* 36(4):735–747
- Matsumura Y, Maeda H (1986) A new concept for macromolecular therapeutics in cancer-chemotherapy-mechanism of tumorotropic accumulation of proteins and the antitumor agent SMANCS. *Cancer Res* 46(12):6387–6392
- Merrill EW, Dennison KA, Sung C (1993) Partitioning and diffusion of solutes in hydrogels of poly(ethylene oxide). *Biomaterials* 14(15):1117–1126
- Mirza AZ, Shamshad H (2011) Preparation and characterization of doxorubicin functionalized gold nanoparticles. *Eur J Med Chem* 46(5):1857–1860. doi:[10.1016/j.ejmech.2011.02.048](https://doi.org/10.1016/j.ejmech.2011.02.048)
- Otsuka H, Nagasaki Y, Kataoka K (2003) PEGylated nanoparticles for biological and pharmaceutical applications. *Adv Drug Deliver Rev* 55(3):403–419. doi:[10.1016/S0169-409x\(02\)00226-0](https://doi.org/10.1016/S0169-409x(02)00226-0)
- Owens DE, Peppas NA (2006) Opsonization, biodistribution, and pharmacokinetics of polymeric nanoparticles. *Int J Pharm* 307(1):93–102. doi:[10.1016/j.ijpharm.2005.10.010](https://doi.org/10.1016/j.ijpharm.2005.10.010)
- Pardo-Yissar V, Gabai R, Shipway AN, Bourenko T, Willner I (2001) Gold nanoparticle/hydrogel composites with solvent-switchable electronic properties. *Adv Mater* 13(17):1320–1323
- Peppas NA, Bures P, Leobandung W, Ichikawa H (2000) Hydrogels in pharmaceutical formulations. *Eur J Pharm Biopharm* 50(1):27–46
- Perala G, Rossi F, Santoro M, Peviani M, Papa S, Llupi D, Torriani P, Micotti E, Previdi S, Cervo L, Sundstrom E, Boccaccini AR, Masi M, Forloni G, Veglianesi P (2012) Multiple drug delivery hydrogel system for spinal cord injury repair strategies. *J Control Release* 159(2):271–280. doi:[10.1016/j.jconrel.2011.12.025](https://doi.org/10.1016/j.jconrel.2011.12.025)
- Phillips JP, Mackey NM, Confait BS, Heaps DT, Deng X, Todd ML, Stevenson S, Zhou H, Hoyle CE (2008) Dispersion of

- gold nanoparticles in UV-cured, thiol-ene films by pre-complexation of gold-thiol. *Chem Mater* 20(16):5240–5245. doi:[10.1021/Cm8007842](https://doi.org/10.1021/Cm8007842)
- Quick DJ, Anseth KS (2004) DNA delivery from photocross-linked PEG hydrogels: encapsulation efficiency, release profiles, and DNA quality. *J Control Release* 96(2):341–351. doi:[10.1016/j.jconrel.2004.01.021](https://doi.org/10.1016/j.jconrel.2004.01.021)
- Ramchandani M, Robinson D (1998) In vitro and in vivo release of ciprofloxacin from PLGA 50:50 implants. *J Control Release* 54(2):167–175. doi:[10.1016/s0168-3659\(97\)00113-2](https://doi.org/10.1016/s0168-3659(97)00113-2)
- Ryman-Rasmussen JP, Riviere JE, Monteiro-Riviere NA (2006) Penetration of intact skin by quantum dots with diverse physicochemical properties. *Toxicol Sci* 91(1):159–165. doi:[10.1093/toxsci/kfj122](https://doi.org/10.1093/toxsci/kfj122)
- Ryman-Rasmussen JP, Riviere JE, Monteiro-Riviere NA (2007) Variables influencing interactions of untargeted quantum dot nanoparticles with skin cells and identification of biochemical modulators. *Nano Lett* 7(5):1344–1348. doi:[10.1021/NI070375j](https://doi.org/10.1021/NI070375j)
- Sukhanova A, Even-Desrumeaux K, Kisserli A, Tabary T, Reveil B, Millot JM, Chames P, Baty D, Artemyev M, Oleinikov V, Pluot M, Cohen JHM, Nabiev I (2012) Oriented conjugates of single-domain antibodies and quantum dots: toward a new generation of ultrasmall diagnostic nanoprobess. *Nanomed-Nanotechnol* 8(4):516–525. doi:[10.1016/j.nano.2011.07.007](https://doi.org/10.1016/j.nano.2011.07.007)
- Taylor A, Krupskaya Y, Kramer K, Fussel S, Klingeler R, Buchner B, Wirth MP (2010) Cisplatin-loaded carbon-encapsulated iron nanoparticles and their in vitro effects in magnetic fluid hyperthermia. *Carbon* 48(8):2327–2334. doi:[10.1016/j.carbon.2010.03.009](https://doi.org/10.1016/j.carbon.2010.03.009)
- Veisoh O, Gunn JW, Kievit FM, Sun C, Fang C, Lee JSH, Zhang MQ (2009) Inhibition of tumor-cell invasion with chlorotoxin-bound superparamagnetic nanoparticles. *Small* 5(2):256–264. doi:[10.1002/sml.200800646](https://doi.org/10.1002/sml.200800646)
- Wang L, Zhang MY, Zhang N, Shi JJ, Zhang HL, Li M, Lu C, Zhang ZZ (2011) Synergistic enhancement of cancer therapy using a combination of docetaxel and photothermal ablation induced by single-walled carbon nanotubes. *Int J Nanomed* 6:2641–2652. doi:[10.2147/Ijn.S24167](https://doi.org/10.2147/Ijn.S24167)
- Watkins AW, Anseth KS (2005) Investigation of molecular transport and distributions in poly(ethylene glycol) hydrogels with confocal laser scanning microscopy. *Macromolecules* 38(4):1326–1334. doi:[10.1021/ma0475232](https://doi.org/10.1021/ma0475232)
- Wohlfart S, Gelperina S, Kreuter J (2012) Transport of drugs across the blood-brain barrier by nanoparticles. *J Control Release* 161(2):264–273. doi:[10.1016/j.jconrel.2011.08.017](https://doi.org/10.1016/j.jconrel.2011.08.017)
- Yezhelyev MV, Qi LF, O'Regan RM, Nie S, Gao XH (2008) Proton-sponge coated quantum dots for siRNA delivery and intracellular imaging. *J Am Chem Soc* 130(28):9006–9012. doi:[10.1021/Ja800086u](https://doi.org/10.1021/Ja800086u)